Article

Discovery Medicine 2024; 36(185): 1199–1209
https://doi.org/10.24976/Discov.Med.202436185.110

MEOX2 Participates in Hepatic Stellate Cells-Induced Liver Fibrosis by Regulating the PI3K/AKT Signaling Pathway

Qiong Wang[1], Ting Li[2], Yansha He[2], Chunyan Rao[2,*]

[1]Department of Gastroenterology, Zi Yang Central Hospital, 641300 Ziyang, Sichuan, China
[2]Department of Liver Disease, Chongqing Traditional Chinese Medicine Hospital, 400021 Chongqing, China
*Correspondence: chunyanrao@126.com (Chunyan Rao)
Published: 20 June 2024

Background: Hepatic stellate cells (HSCs) serve as the crucial accelerating factor in the progression of liver fibrosis (LF). In contrast to HSCs, adult-derived human liver stem/progenitor cells (ADHLSCs) exhibit greater potency in terms of differentiation and proliferation, rendering them highly applicable in LF treatment. The objective of this study is to identify new therapeutic targets for LF by comparing differentially expressed genes (DEGs) between ADHLSCs and HSCs.
Methods: We investigated DEGs between ADHLSCs and HSCs using the GSE49995 dataset obtained from the Gene Expression Omnibus (GEO) database, aiming to identify new therapeutic targets for LF. Subsequently, we activated HSCs to delve deeper into the mesenchyme homeobox 2 (MEOX2), PH domain Leucine-rich repeat protein phosphatase (PHLPP), and Phosphoinositide 3-kinase (PI3K)/protein kinase B (AKT) signaling pathways in LF progression, employing platelet-derived growth factor (PDGF), and conducted infection with Overexpression (OE)-*MEOX2* and shRNA-*MEOX2* (sh-*MEOX2*) lentiviruses. Cell viability was assessed using the Cell Counting Kit-8 (CCK-8) assay, while cell proliferation was evaluated through 5-ethynyl-2′-deoxyuridine (EdU) staining and flow cytometry. Relative mRNA expression levels were determined via qPCR. Western blot analysis was performed to measure protein expression levels, and the regulatory role of MEOX2 was investigated using dual luciferase reporter assays.
Results: We identified 332 DEGs that were down-regulated and 201 DEGs that were up-regulated between ADHLSCs and HSCs. Notably, *MEOX2* expression in ADHLSCs was significantly reduced. These DEGs primarily participated in the collagen-containing extracellular matrix and the PI3K/AKT signaling pathway. MEOX2 could inhibit cancer cell proliferation via the PI3K/AKT signaling pathway. Additionally, the JASRPAR2022 database predicted the target gene *PHLPP* of MEOX2. Our results indicated that OE-*MEOX2* significantly inhibited HSCs' cell vitality and proliferation. Further analysis revealed that MEOX2 binds to *PHLPP* promoters, thereby up-regulating its transcription. This action led to the inhibition of p-AKT expression, consequently reducing HSC proliferation and slowing the progression of LF.
Conclusions: MEOX2 up-regulates PHLPP expression and inhibits AKT phosphorylation, thereby reducing the cell activity and proliferation ability of HSCs and inhibiting the progression of LF.

Keywords: liver fibrosis; hepatic stellate cells; bioinformatics analysis; MEOX2; PI3K/AKT; PHLPP

Introduction

A fibrous scar develops when excess diffuse extracellular matrix (ECM), particularly collagen, is deposited in the liver following liver fibrosis (LF) [1,2]. This fibrotic scar has the potential to damage liver structure, leading to aberrant liver function and homeostasis, ultimately culminating in liver failure [3,4]. In addition to cirrhosis and liver cancer, LF is implicated in hepatic encephalopathy and liver failure. Liver cirrhosis and liver cancer collectively contribute to 3.5% of global deaths annually [5]. LF, being a reversible process, can be reversed as long as it has not progressed to advanced cirrhosis [6].

Adult-derived human liver stem/progenitor cells (ADHLSCs) and hepatic stellate cells (HSCs) reside in the parenchymal and non-parenchymal regions of the liver, respectively. While ADHLSCs share similar cell morphology and surface markers with HSCs activated during liver injury, their gene expression and secretion profiles exhibit significant differences. Both Mesenchymal stromal/stem cells (MSCs) and ADHLSCs demonstrate similar expression profiles, belonging to a class of stem cells characterized by self-renewal and differentiation potential [7,8]. In comparison to HSCs, ADHLSCs possess enhanced proliferation capabilities and can secrete growth factors, pro-/anti-inflammatory factors, and anti-fibrosis-related factors. These contribute to liver tissue regeneration and hinder fi-

brosis development [9]. Conversely, activated HSCs in the injured liver exhibit expression profiles closely associated with proliferation, contraction, fibrogenesis, and chemotaxis, serving as pivotal initiators of LF [10,11].

In this study, Gene Expression Omnibus (GEO) datasets comparing the expression profiles of ADHLSCs and HSCs were utilized, and the differentially expressed genes between these cell types were analyzed. Notably, the expression of mesenchyme homeobox 2 (*MEOX2*) in ADHLSCs was significantly down-regulated compared to HSCs. Previous research suggests that MEOX2 suppresses the proliferation of laryngeal carcinoma cells by inhibiting the Phosphoinositide 3-kinase (PI3K)/protein kinase B (AKT) signaling pathway [12], which might contribute to the heightened proliferation capacity of ADHLSCs relative to HSCs. MEOX2 functions as a transcription factor, and predictions from the JASRPAR2022 database indicate that PH domain Leucine-rich repeat protein phosphatase (*PHLPP*) may be a target gene of MEOX2, subject to transcriptional regulation by MEOX2 protein. Additionally, earlier studies have demonstrated that PHLPP overexpression inhibits colon cancer cell proliferation through AKT dephosphorylation [13,14].

Therefore, we hypothesized that MEOX2 may play a role in HSC proliferation and the promotion of fibrosis following activation. This study was initiated to explore the relationship and underlying mechanism between MEOX2 and HSC proliferation, as well as the pro-fibrotic phenotype, at the cellular level. We employed molecular biological techniques, including gene regulation and dual-luciferase reporter gene detection, to investigate these mechanisms. Our aim is to identify new therapeutic targets and establish a theoretical framework for the management of LF.

Methods

Data Acquisition

GSE49995 is a dataset obtained from NCBI's GEO database (https://www.ncbi.nlm.nih.gov/geo/), which contains a comparison of the expression profiles of ADHLSCs and HSCs.

Differential Genes Analysis

In this section, we utilized the Limma package from R software (version 4.1.2, R Foundation for Statistical Computing, Vienna, Austria) to perform the analysis of the downloaded data. Differential analysis was conducted, and multiple hypothesis testing was employed to calculate the *p*-value and correct it. The threshold for the *p*-value was determined by controlling the false discovery rate (FDR), and the corrected *p*-value, known as the Q-value, was obtained. Additionally, based on the Fragments per kilobase of transcript per million mapped reads (FPKM) value, we calculated the differential expression Fold (fold-change) and analyzed the screening criteria for significance, considering a *p*-value < 0.05 and a $\log_2 |\text{Fold Change}| > 1$.

Gene Ontology (GO) and Kyoto Encyclopedia of Genes and Genomes (KEGG) Enrichment Analyses

Functional enrichment analysis of the fetched differential genes was conducted using the database for annotation, visualization and integrated discovery (DAVID) (https://david.ncifcrf.gov/), an online tool. Additionally, an enrichment analysis through KEGG pathways was carried out using KEGG orthology based annotation system (KOBAS) (http://kobas.cbi.pku.edu.cn/) to determine KEGG pathway enrichment. Subsequently, the enrichment analysis results were visualized using a bubble diagram.

Lentivirus Transfection

The *MEOX2* overexpression and interference lentiviral vectors (shRNA-*MEOX2*) were designed and constructed by Chongqing Biomedicine Biotechnology Co., Ltd., Chongqing, China. The sequence of the interference target sites is presented in Table 1. In brief, a chemically synthesized oligonucleotide encoding the *MEOX2* overexpression sequence was subcloned into the EcoRI and NotI sites of the lentiviral expression vector pLVX-IRES-puro. Similarly, a chemically synthesized oligonucleotide encoding the *MEOX2* shRNA sequence was subcloned into the BamHI and EcoRI sites of pLVX-shRNA1. These constructs were then transfected into 293T cells, and viral particles were harvested 48 hours later.

Cell Culture and Grouping

We acquired LX-2 HSCs from Procell LifeScience & Technology (Wuhan, China). The cultures were maintained in an incubator at 37 °C with 5% CO_2 using dulbecco's modified eagle medium (DMEM) complete medium comprising 10% fetal bovine serum (FBS) and 1% penicillin-streptomycin. Cells were seeded at a density of 1×10^5 cells per mL in 10-well plates, and the treatment groups were administered the following day. The control group was cultured with DMEM complete medium for 72 hours.

In the platelet-derived growth factor (PDGF) group, cells were cultured for 72 hours in complete medium supplemented with 10 ng/mL PDGF (HY-P7055, MedChemExpress, Shanghai, China). For the Overexpression (OE)-*MEOX2*+PDGF group, cells were incubated in an incubator containing 30 mL of overexpressed lentivirus suspension (1×10^8 TU/mL) and 5 g/mL polybrene (C051-50mg, Beyotime, Shanghai, China) for 48 hours. Following this, the culture medium was replaced with a complete medium containing 10 ng/mL PDGF for an additional 24 hours. In the shRNA-*MEOX2* (sh-*MEOX2*)+PDGF group, a medium containing 30 mL interfering lentivirus suspension was added for 48 hours, and then the medium was changed to a complete medium containing 10 ng/mL PDGF for 24 hours. The identification of all cell lines was performed using short tandem repeat (STR) profiling, confirming the absence of mycoplasma contamination.

Table 1. Sequence of interfering target sites.

Target site	Sequence
MEOX2-oligo	GCATTTCTCCAAGGACTTTGA
Top Strand	5′-GGGCATTTCTCCAAGGACTTTGACTCGAGTCAAAGTCCTTGGAGAAATGCTTTTTTG-3′
Bottom Strand	5′-GATTCAAAAAAGCATTTCTCCAAGGACTTTGACTCGAGTCAAAGTCCTTGGAGAAATGCCCTGCA-3′

Note: The Loop Sequence in shRNA was CTCGAG. *MEOX2*, mesenchyme homeobox 2.

CCK-8 Assay

The cells were harvested 72 hours after treatment, and the culture medium was removed. PBS was then added to the cells, and the wells were replenished with fresh medium containing 10% Cell Counting Kit-8 (CCK-8) solution (C0038, Beyotime, Shanghai, China). Subsequently, the plates were incubated for 4 hours, and the absorbance was measured at 450 nm using a UV-Vis microspectrophotometer (NanoDrop One/One C, Thermo Fisher Scientific, Waltham, MA, USA). Wells designated as blanks contained only medium and CCK-8 solution, while control wells contained cells, medium, and CCK-8 solution.

EdU Staining

Add preheated 5-ethynyl-2′-deoxyuridine (EdU) solution at 37 °C in an equal volume to a 6-well plate and incubate the cells for 2 hours. Afterward, remove the culture medium and add 1 mL of 4% paraformaldehyde fixing solution (DF0135, Leagene, Beijing, China), allowing the cells to be fixed at room temperature for 15 minutes. Subsequently, remove the fixative and wash the cells with 1 mL of PBS three times, with each wash lasting 3 to 5 minutes.

Next, remove the PBS and add 1 mL of permeabilization solution (PBS with 0.3% Triton X-100 (ST795, Beyotime, Shanghai, China)) to each well, followed by incubation at room temperature for 10 to 15 minutes. Afterward, remove the permeabilization solution and wash the cells with 1 mL of washing solution 1 to 2 times per well, with each wash lasting 3 to 5 minutes.

Following the washing steps, add 0.5 mL of Click solution (Formulated by Click solution, CuSO4, Azide 488, and Click Additive Solution) to each well and gently shake the culture plate to ensure even coverage of the reaction mixture. Incubate the plate at room temperature for 30 minutes, away from light.

After incubation, remove the Click reaction solution and wash the cells with PBS three times, for 3 to 5 minutes each time. Once the PBS has been absorbed, add 1 mL of 2-(4-Amidinophenyl)-6-indolecarbamidine dihydrochloride (DAPI) staining solution (C1006, Beyotime, Shanghai, China) to each well and incubate at room temperature for 10 minutes, away from light.

Finally, remove the DAPI staining solution and wash the cells with PBS three times, with each wash lasting 3 to 5 minutes each time. The cells are now ready for fluorescence detection.

Flow Cytometry

Add preheated EdU solution at 37 °C in an equal volume to a 6-well plate and incubate the cells for 2 hours. After incubation, remove the culture medium and gently detach the cells, then resuspend them in the medium. Subsequently, add 1 mL of 4% paraformaldehyde fixing solution (DF0135, Leagene, Beijing, China) to each tube and fix the cells at room temperature for 15 minutes.

Once fixed, remove and wash each tube with 1 mL of PBS three times, with each wash lasting 3 to 5 minutes. Following the PBS washes, remove the PBS and add 1 mL of permeabilization solution to each tube, then incubate at room temperature for 10 to 15 minutes. After incubation, remove the permeabilization solution and wash the cells with 1 mL of washing solution 1 to 2 times, with each wash lasting 3 to 5 minutes. Next, add 0.5 mL of Click solution to each tube and gently shake to ensure even coverage of the reaction mixture. Incubate the tubes at room temperature for 30 minutes, away from light. After incubation, remove the Click reaction solution and wash the cells with PBS three times, with each wash lasting 3 to 5 minutes each time. Once the PBS has been absorbed, add 200 µL of buffer to each well, and incubate at room temperature for 10 minutes, away from light. Following this, perform flow cytometry using a Flow cytometer (Beamcyte-1026M, Betalco, Changzhou, China).

Quantitative Real-Time Reverse-Transcription PCR (qRT-PCR)

Total RNA was extracted from each group of cells using the TRIzol method (15596-018, Thermo Fisher Scientific, Waltham, MA, USA). Subsequently, cDNA synthesis was performed according to the Goldenstar™ RT6 cDNA Synthesis Kit Ver.2 (TSK302M, Tsingke, Beijing, China).

For quantitative PCR (qPCR), the reaction system was prepared with reference to the 2×T5 Fast qPCR Mix (SYBR Green I) kit (TSE002, Tsingke, Beijing, China), and then the reaction was carried out in a real-time fluorescence quantitative PCR instrument (7500, Bio-Rad, Hercules, CA, USA). Relative quantitative analysis of *MEOX2*, α-smooth muscle actin (α-*SMA*), *PI3K*, and *AKT* was conducted using the $2^{-\Delta\Delta Ct}$ method, with the expression of glyceraldehyde-3-phosphate dehydrogenase (*GAPDH*) serving as a reference. The primer sequences used are shown in Table 2.

Relative expression calculation method:

ΔCt (experimental group) = Ct (target gene of experimental group) – Ct (reference gene of experimental group)

ΔCt (control group) = Ct (target gene of control group) – Ct (reference gene of control group)

$\Delta\Delta$Ct = ΔCt (experimental group) – ΔCt (control group)

The relative expression level is $2^{-\Delta\Delta Ct}$ (denotes the fold change of the target gene expression in the experimental group compared with the control group).

Table 2. Primer sequence.

Primer name	Sequence (5′ to 3′)
MEOX2-F	CTCTGCAAACCAACTGGCAC
MEOX2-R	AAGAGTTGGAGCACAGGACG
α-*SMA*-F	GACATCAGGGGGTGATGGTG
α-*SMA*-R	CAGGGTGGGATGCTCTTCAG
PI3K-F	GCGCAAATTCAGCGAGGAAA
PI3K-R	ACACGTCCTGGCAGTTTTCA
AKT-F	GCACAAACGAGGGGAGTACA
AKT-R	AAGGTGCGTTCGATGACAGT
GAPDH-F	GCAAGTTCAACGGCACAG
GAPDH-R	GCCAGTAGACTCCACGACATA
PHLPP-F	GTTGCATCCCAGCGCATTAG
PHLPP-R	AGTTCATTAAGCCCCCTGGC

α-*SMA*, α-smooth muscle actin; *PI3K*, Phosphoinositide 3-kinase; *AKT*, protein kinase B; *GAPDH*, glyceraldehyde-3-phosphate dehydrogenase; *PHLPP*, PH domain Leucine-rich repeat protein phosphatase; F, Forward primer; R, Reverse primer.

Western Blot

Total cellular proteins were extracted using radio immunoprecipitation assay (RIPA) lysis buffer (containing phenylmethanesulfonylfluoride or phenylmethylsulfonyl fluoride (PMSF) and protease inhibitor cocktail) (P0013B, Beyotime, Shanghai, China) and denatured by heating at 100 °C for 6 minutes. Subsequently, 60 µg of denatured total protein was loaded for sample loading, and electrophoresis was performed at 80 V initially, followed by conversion to 120 V. Electrophoresis continued until the bromophenol blue dye migrated to the bottom of the gel without running off. The current was adjusted to a constant of 250 mA, and the transfer time was determined based on the molecular weight of the proteins.

After electrophoresis, membranes were blocked in a 5% skim milk solution at room temperature for 2 hours. Following blocking, the membranes were incubated with the corresponding primary antibodies (1:1000 dilution) overnight at 4 °C. Subsequently, the membranes were washed three times with TBST before being incubated with secondary antibodies (1:2000 dilution) for one hour at room temperature. After washing with TBST, the enhanced chemiluminescence (ECL) exposure solution was prepared by mixing solution A and solution B at a 1:1 ratio, and the entire membrane was evenly covered with the mixture. Protein bands were detected using a nucleic acid protein gel imager (Universal Hood II, Bio-Rad, Hercules, CA, USA).

Finally, ImageJ 1.53 software (National Institutes of Health, Bethesda, MD, USA) was utilized to analyze the gray values of the protein bands, allowing the determination of the expressions of MEOX2, α-SMA, PI3K, AKT, P-PI3K, and p-AKT. The relative gray value was calculated as the ratio of the assayed gray value of the protein to the internal reference gray value of GAPDH. Primary antibodies MEOX2 (AB124876), α-SMA (A17910), PI3K (A0265), AKT (A11016), P-PI3K (AP0854), P-AKT (AP0637), and GAPDH (A19056) were procured from Abclonal (Wuhan, China).

Dual-Luciferase Reporter Gene Assay

The 2000 bp sequence of the promoter region of the *PHLPP* gene was synthesized and cloned into a pGL4.11-Basic vector, designated as pGL4.11-WT. Additionally, the binding site within the 2000 bp sequence of the *PHLPP* promoter region was mutated, synthesized, and cloned into the vector, denoted as pGL4.11-mut.

To transfect the plasmids into cells, 50 µL of culture medium without antibiotics and serum was added to each well. Then, 1 µg of plasmid (group mixed) was gently mixed with a pipette. Subsequently, 1.6 µL of Nanofusion transfection reagent was added, and the mixture was gently mixed again. The mixture was allowed to sit at room temperature for 5 to 20 minutes before being added to cells in 12-well plates. After 48 hours, the luciferase relative activity was measured according to the instructions provided with the dual luciferase detection kit (E1483, Promega, Madison, WI, USA).

Statistic Analysis

All test results were replicated three times, and statistical analysis was performed using Prism GraphPad 9.0 software (GraphPad Software, La Jolla, CA, USA). One-way analysis of variance (ANOVA) analysis and graphical representation were conducted. Tukey's post hoc test was utilized for multiple comparisons. Statistical significance was defined as $p < 0.05$. Data were presented as mean $\pm$ standard deviation.

Result

Election and Enrichment Analysis of DEGs

Based on the screening index with a threshold of p-value < 0.05 and $|\log_2$ Fold Change$| > 1$, a total of 533 differential genes were identified. Among them, 332 genes were found to be down-regulated, while 201 genes were

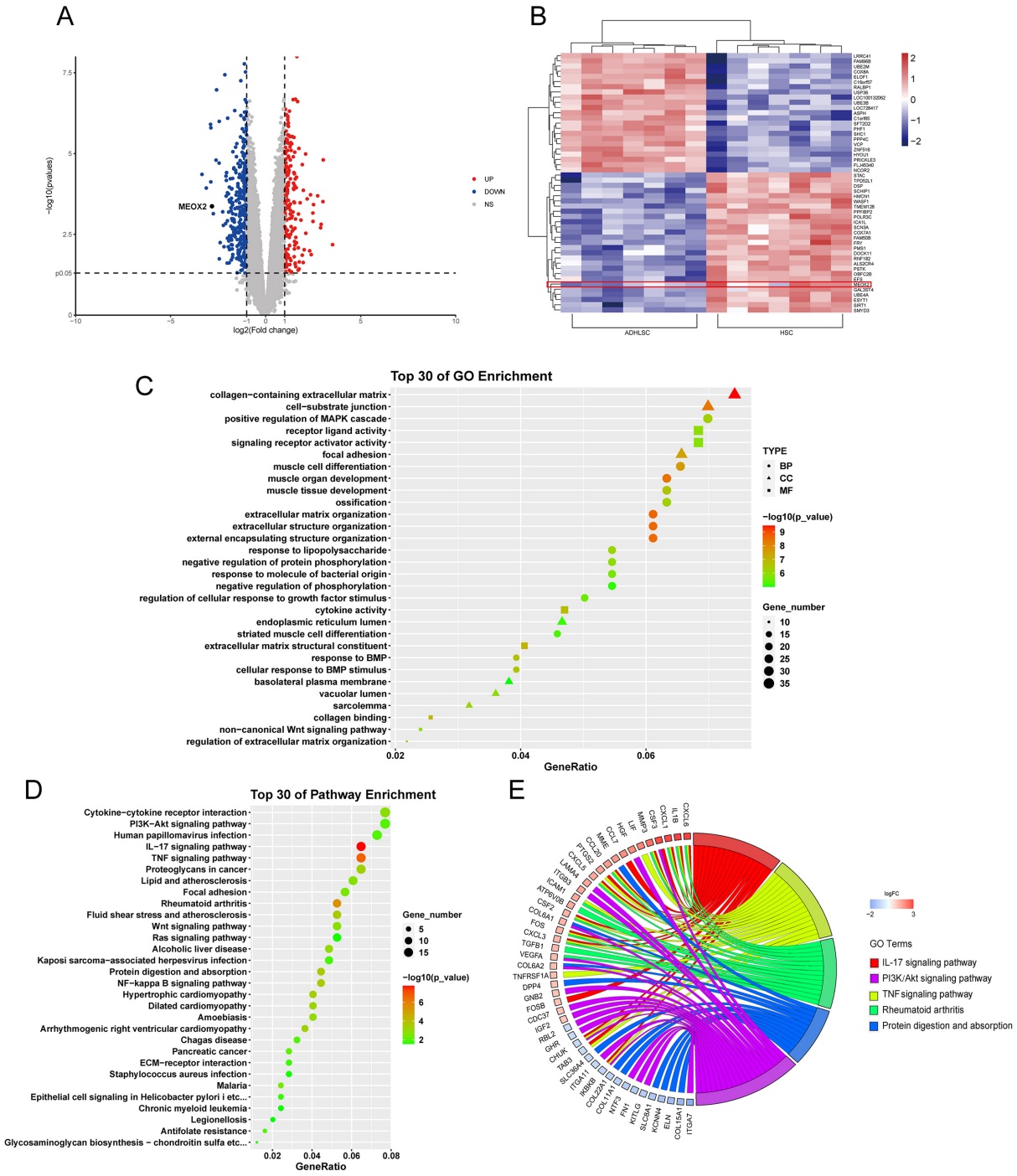

Fig. 1. DEGs analysis of ADHLSCs and HSCs based on the GSE49995 dataset of the GEO database. (A) DEGs volcano map. (B) Heat map of Top 50 DEGs. (C) Top 30 items for GO enrichment analysis of DEGs. (D) Top 30 items for KEGG enrichment analysis of DEGs. (E) Chordal graph of KEGG enrichment analysis. DEGs, differentially expressed genes; ADHLSCs, adult-derived human liver stem/progenitor cells; HSCs, hepatic stellate cells; GEO, Gene Expression Omnibus; GO, Gene Ontology; KEGG, Kyoto Encyclopedia of Genes and Genomes.

up-regulated (Fig. 1A). Additionally, a heatmap illustrating the expression patterns of the top 50 differentially expressed genes (DEGs) was generated. Furthermore, within ADHLSCs, 27 genes were up-regulated, whereas 23 genes were down-regulated (Fig. 1B).

Following the identification of DEGs, we conducted Gene Ontology (GO) enrichment analysis and Kyoto Encyclopedia of Genes and Genomes (KEGG) enrichment analysis. The GO enrichment analysis revealed significant findings across various categories. Specifically, in terms of cellular components (CC), notable orders included

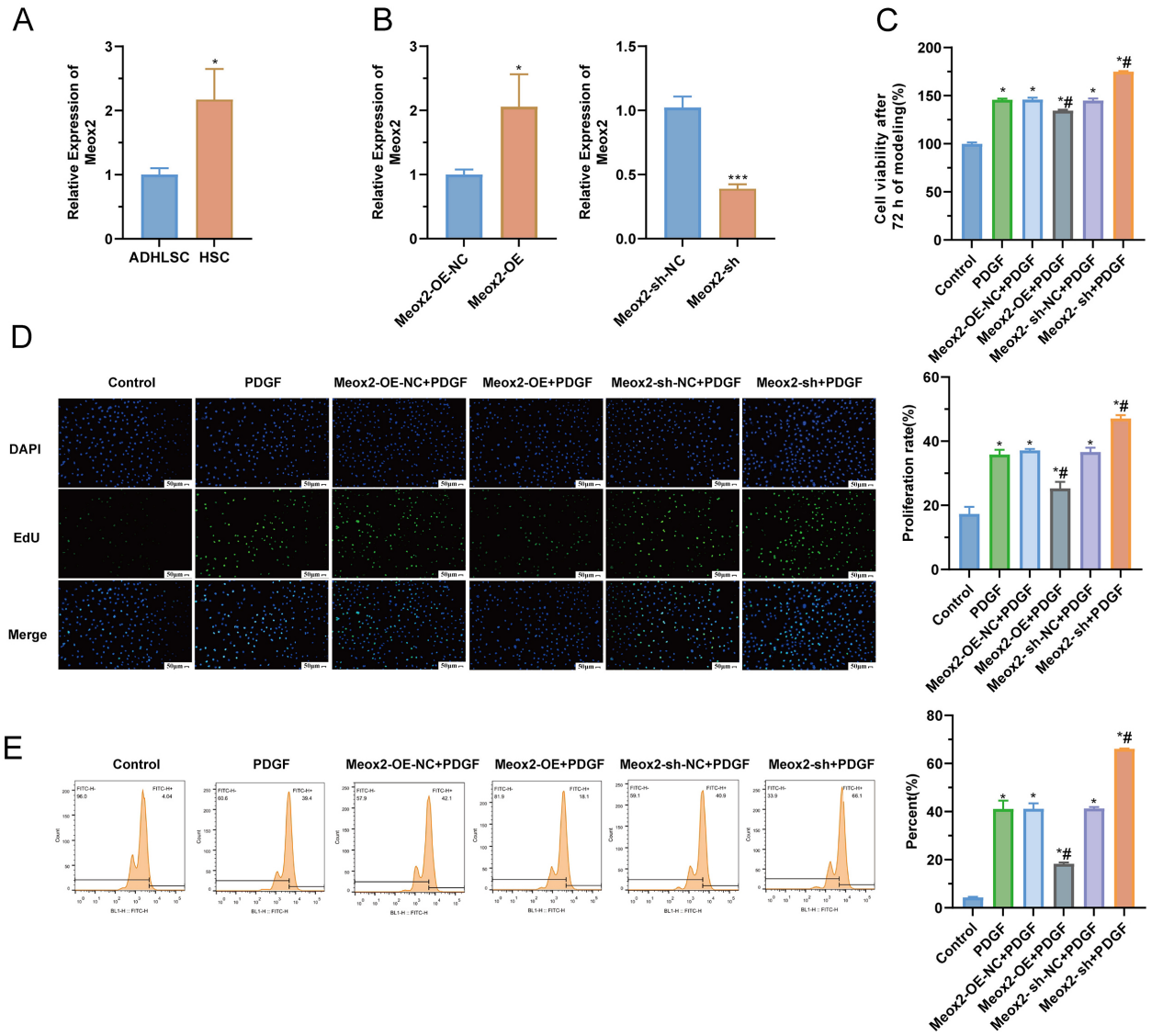

Fig. 2. Effect of MEOX2 on PDGF-induced HSCs viability and proliferation. (A) Basic expression of *MEOX2*. (B) *MEOX2* transfection efficiency. (C) CCK-8 assay to detect the effect of MEOX2 on HSCs viability. (D,E) EdU staining and flow cytometry to detect the effect of MEOX2 on HSCs proliferation. n = 3, * $p < 0.05$ *vs* Control, *** $p < 0.001$ *vs* Control, $^{\#}$ $p < 0.05$ *vs* PDGF. PDGF, platelet-derived growth factor; CCK-8, Cell Counting Kit-8; EdU, 5-ethynyl-2′-deoxyuridine.

the collagen-containing extracellular matrix, cell-substrate junctions, and focal adhesions. Molecular function (MF) analysis encompassed receptor ligand activity, signaling receptor activator activity, and cytokine activity. Additionally, biological processes (BP) comprised positive regulation of mitogen-activated protein kinase (MAPK) cascade, extracellular matrix organization, and muscle cell differentiation (Fig. 1C).

Moreover, KEGG enrichment analysis highlighted several signaling pathways associated with the identified differential genes. Predominant pathways included cytokine receptor interaction, PI3K-AKT signaling pathway, human papillomavirus pathway, IL-17 signaling pathway, and tumor necrosis factor (TNF) signaling pathway (Fig. 1D).

Based on these results, we aimed to validate the significance of the *MEOX2* gene ($\log_2$FC = –2.82501, p = 0.000428) and its potential involvement in the PI3K/AKT signaling pathway. Existing literature has demonstrated *MEOX2*'s role in regulating cell proliferation, differentiation, and apoptosis through the PI3K/AKT pathway [12, 15]. However, contrary to expectations, *MEOX2* was not implicated in the PI3K/AKT signaling pathway according to the KEGG enrichment analysis results of this study (Fig. 1E). Therefore, subsequent cellular validation experiments are warranted.

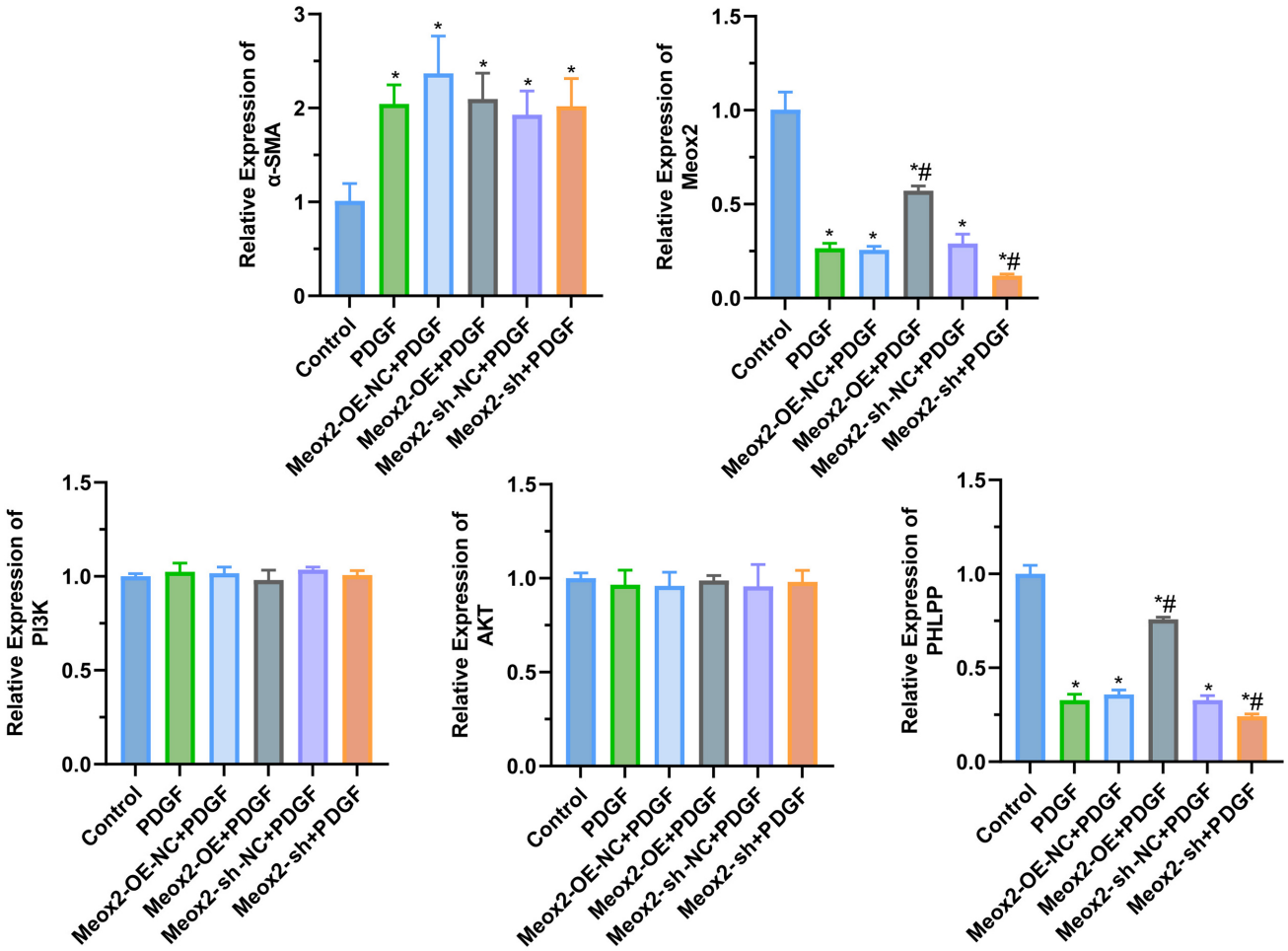

Fig. 3. qRT-PCR was performed to detect the effect of *MEOX2* on the relative mRNA expression of α-*SMA*, *PI3K*, *AKT*, and *PHLPP*. * $p < 0.05$ *vs* Control, $^{\#}$ $p < 0.05$ *vs* PDGF. qRT-PCR, quantitative real-time reverse-transcription PCR; *PHLPP*, PH domain Leucine-rich repeat protein phosphatase.

Effect of MEOX2 on the Activity and Proliferation of HSCs

The basal expression of *MEOX2* was verified through qPCR, revealing significantly higher expression levels in HSCs compared to ADHLSCs (Fig. 2A), consistent with the findings from bioinformatics analysis. To explore the impact of *MEOX2* on cell viability and proliferation, HSCs were induced with 10 ng/mL PDGF. Lentiviruses carrying OE-*MEOX2* and sh-*MEOX2* constructs were employed for cell infection (Fig. 2B).

Subsequently, assays including CCK-8, EdU, and flow cytometry were conducted to investigate the effect of MEOX2 on cell viability and proliferation. The CCK-8 results demonstrated a significant increase in cell viability following PDGF treatment compared to the control group. Notably, the OE-*MEOX2*+PDGF group exhibited a significant decrease, whereas the sh-*MEOX2*+PDGF group showed a significant increase in cell viability compared to the PDGF group ($p < 0.05$, Fig. 2C).

In the EdU assay, total nuclei were stained blue, while proliferating cells were stained green (Fig. 2D). The percentage of EdU-labeled positive cells, representing proliferation, was indicated in the upper right corner of the flow cytometry results (Fig. 2E). PDGF treatment led to a notable increase in cell proliferation ability ($p < 0.05$, Fig. 2C–E). Additionally, compared to the PDGF group, the OE-*MEOX2*+PDGF group exhibited a significant decrease in proliferation ability, whereas the sh-*MEOX2*+PDGF group showed a significant increase (Fig. 2D,E).

These findings suggest that overexpression of *MEOX2* attenuates PDGF-induced cell proliferation and fibrosis, while interference with *MEOX2* promotes cell viability and proliferation.

Effects of MEOX2 on the Expression of α-SMA, PI3K, AKT and PHLPP

Compared to the control group, PDGF significantly promoted the expression of α-*SMA* while decreasing the expression of *MEOX2* and *PHLPP*. However, there was no significant effect on the expression of *PI3K* and *AKT*. Moreover, compared to PDGF alone, OE-*MEOX2* upregulated the expression of *PHLPP*, whereas sh-MEOX2

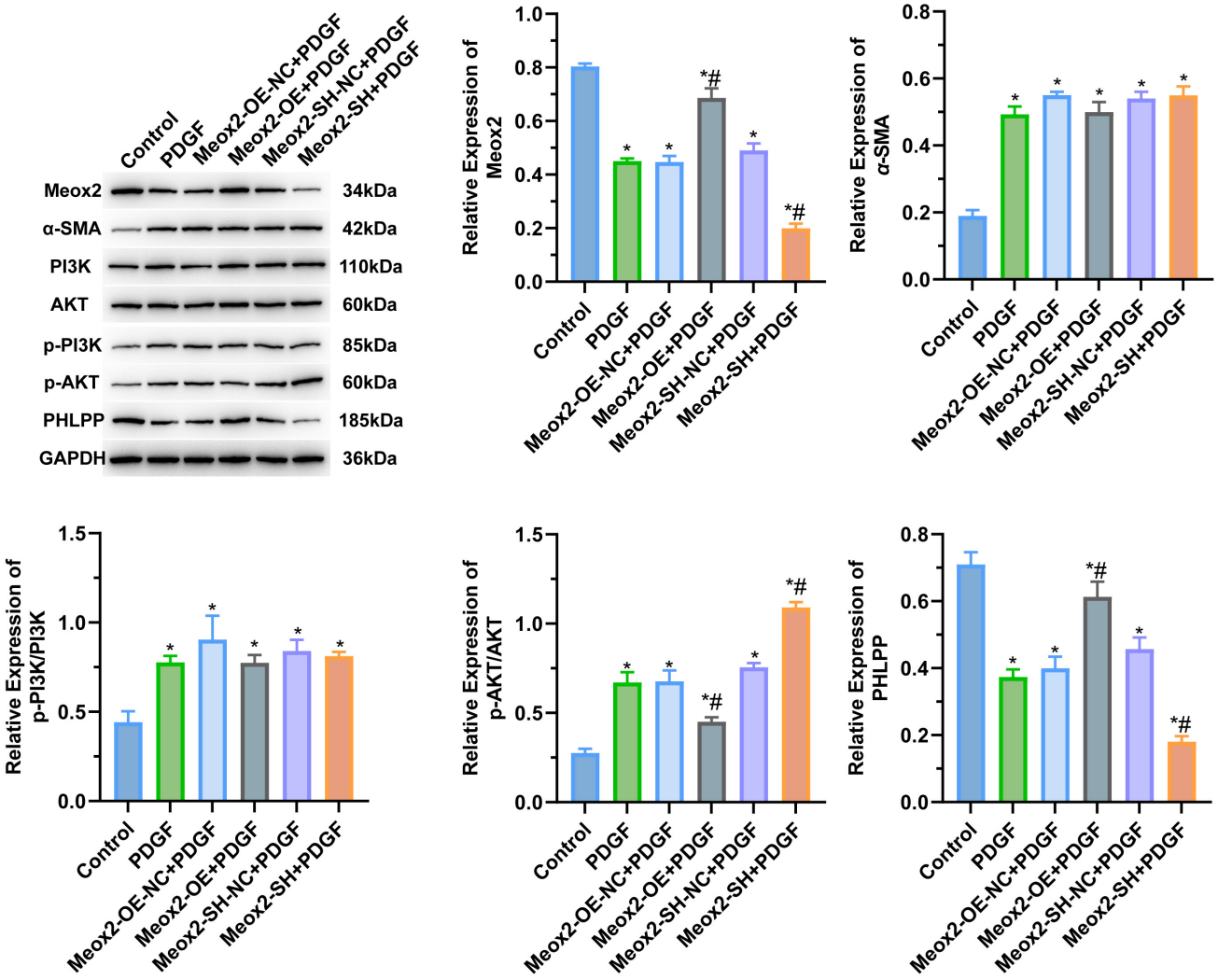

Fig. 4. Western blot was performed to detect the effect of MEOX2 on the relative protein expression of α-SMA, PI3K, AKT, p-AKT, p-PI3K, and PHLPP. * $p < 0.05$ *vs* Control, # $p < 0.05$ *vs* PDGF.

down-regulated it (Fig. 3), indicating a regulatory role of *MEOX2* on *PHLPP* expression. The results obtained from western blot analysis corroborated those from qRT-PCR. Notably, the expression of p-PI3K/PI3K was significantly increased by PDGF compared to the control group. Additionally, the expression of p-AKT was regulated by *MEOX2*, decreasing with *MEOX2* overexpression (Fig. 4). These findings suggest that overexpression of *MEOX2* activates phosphorylated AKT and regulates PHLPP expression.

Results of Double Luciferase Reporter Gene

Through dual luciferase reporter gene assays, we investigated the regulatory effect of *MEOX2* and its binding site on *PHLPP*. The results revealed that co-transfection of *MEOX2* and PGL4.11-WT significantly increased the relative fluorescence intensity compared to the control group. Conversely, co-transfection of *MEOX2* and pGL4.11-MUT led to significantly lower fluorescence intensity compared to the *MEOX2*+pGL4.11-WT group (Fig. 5). These findings suggest that *MEOX2* possesses a binding site within the *PHLPP* promoter region and up-regulates the expression of *PHLPP*.

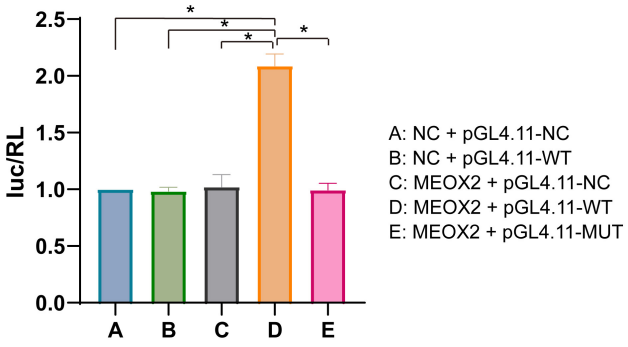

Fig. 5. Dual-luciferase reporter gene assay was performed to detect the binding sites of *MEOX2* to *PHLPP*. * $p < 0.05$.

Discussion

LF is a pathological condition characterized by an inflammatory response and excessive accumulation of ECM in the liver due to various acute and chronic liver injury factors. Although effective therapeutic strategies directly targeting and reversing advanced LF are currently lacking, clinical studies have demonstrated the potential for LF resolution through interventions targeting the underlying etiology.

HSCs play a pivotal role in LF progression. Upon liver injury, HSCs become activated and secrete abundant ECM, matrix metalloproteinases, and tissue inhibitors of metalloproteinases. Interactions between liver cells, liver sinusoidal endothelial cells, and Kupffer cells further contribute to elevated LF levels, resulting in fibrous deposition, liver tissue remodeling, and acceleration of LF progression [16].

Under normal circumstances, HSCs remain quiescent. However, they can be activated directly or indirectly by various factors, including hepatic epithelial cell and inflammatory cell injury, the fibrotic tissue microenvironment, immune and systemic metabolic disorders, intestinal microecological imbalances, and paracrine signals produced by hepatitis virus products in response to acute or chronic liver damage [17].

Activated HSCs differentiate into myofibroblasts, which exhibit robust proliferation, migration, and secretion capabilities [18]. Continued LF development can lead to liver cirrhosis and potentially liver cancer, resulting in severe complications such as portal hypertension, liver failure, hepatic encephalopathy, ascites, and other serious diseases [19].

It is widely acknowledged that inhibiting the activation and proliferation of HSCs, inducing senescence and apoptosis of activated HSCs, and promoting their clearance hold promise for reversing LF progression.

There is a robust correlation between the occurrence of LF and the PDGF signaling pathway. PDGF, a polypeptide growth factor, is primarily secreted by Kupffer cells, platelets, and vascular endothelial cells [20]. It is also expressed in HSCs. PDGF converts hematopoietic stem cells into myofibroblasts by promoting collagen production and deposition, thereby stimulating HSC proliferation and differentiation [21]. Consequently, blocking PDGF signaling can inhibit HSC proliferation and improve LF. Loss of PDGF receptor α (PDGFRα) in hepatocytes attenuates PDGFRα upregulation in HSCs, thereby reducing LF and HSC activation [22].

Studies have demonstrated that inhibiting the PDGF-B/PDGFR-β pathway in HSCs can ameliorate LF in cholestatic mice [23]. Additionally, the synthesis of PDGFR-β is linked to the PI3K/AKT signaling pathway. PI3K inhibitors Wortmannin and LY294002 can impede the expression of PDGFR-β [24]. Wang *et al*. [25] investigated the anti-fibrotic effects of sorafenib (targeted PDGF receptor inhibition) and found that sorafenib inhibited HSC proliferation and reduced collagen synthesis by suppressing AKT and p70S6K phosphorylation. Chen *et al*. [26] observed that gypenosides inhibited PDGF-induced HSC proliferation and activation by suppressing the PDGF-PI3K/AKT-p70S6K signaling pathway.

It appears that the PI3K/AKT signaling pathway plays a crucial role in PDGF receptor expression. α-SMA, as a constituent of the extracellular matrix, is involved in the synthesis of collagen type I, collagen type III, fibronectin, and other extracellular matrix components. In the current study, PDGF significantly promoted HSC proliferation and α-SMA expression levels, indicating successful HSC activation. While MEOX2 does not exert a significant impact on α-SMA expression, this does not necessarily imply that MEOX2 has no role in the sustained activation of HSCs. The regulation of α-SMA expression is a complex process involving multiple signaling pathways and factors. For instance, Cunnington *et al*. [27] discovered that Ski inhibits Zeb2 protein expression by an unknown mechanism, thereby restoring MEOX2 expression and reducing α-SMA secretion. Further exploration of these mechanisms is necessary for future research.

A growth lag-specific homeobox protein known as MEOX2 regulates both cell proliferation and differentiation. MEOX2 controls these processes by regulating the protein-dependent kinase P21wafl, thereby upregulating its expression [28,29]. The expression pattern of MEOX2 in tumor cells is highly specific and closely associated with tumor development and prognosis. Moreover, increasing the expression of the *MEOX2* gene can induce apoptosis and inhibit the proliferation of cancer cells [30]. MEOX2 expression inhibits the activation of the PI3K/AKT1 pathway and promotes apoptosis in perivascular adipocytes and renal cancer cells [12,15]. Consequently, MEOX2 has been identified as a novel target for cancer and vascular lesions.

The leucine-rich repeat protein phosphatase (*PHLPP*) gene is located on chromosomes 18 and 16. The protein phosphatase PHLPP, encoded by the *PHLPP* gene, phosphorylates AKT and diminishes its protease activity, thereby inhibiting the cell growth-promoting effect of AKT. PHLPP exhibits widespread expression in various tissues, organs, and cells of the human body. Analysis of the molecules and biochemical composition of human tumor cells has revealed a significant reduction in the level of PHLPP in several tumor types (e.g., colon cancer), accompanied by a notable increase in phosphorylation levels of AKT. This observation suggests that the PHLPP protein acts as a negative regulator of tumor growth [31]. Consequently, PHLPP, as a tumor suppressor, holds promise for the treatment of all cancers associated with elevated AKT levels.

In this study, qRT-PCR and western blot analyses were employed to investigate the effects of *MEOX2* on the PI3K/AKT pathway and PHLPP. Our findings demon-

strate that over-expression of *MEOX2* upregulates PHLPP expression while downregulating p-AKT expression. Furthermore, we observed that *MEOX2* binds to the promoter region of *PHLPP*, indicating that *MEOX2* regulates *PHLPP* transcription and AKT phosphorylation. Consequently, we have reasonable grounds to consider MEOX2 as a potential treatment target for LF.

Conclusions

The aforementioned results indicate that *MEOX2* has the capability to hinder the activation of p-AKT by increasing the transcription of *PHLPP*, consequently diminishing the cellular activity of HSCs and impeding the progression of LF. Our experimental findings suggest that MEOX2 holds promise as a potential treatment target for LF, offering a novel avenue for prevention and treatment strategies.

Availability of Data and Materials

All data, models, and code generated or used during the study appear in the submitted article.

Author Contributions

QW and CR designed the study. QW, TL and YH performed the research. TL and YH analyzed the data. CR provided funding support and acquired the data. All authors were involved in drafting and critical revision of the manuscript. All authors read and approved the final manuscript. All authors have participated sufficiently in the work and agreed to be accountable for all aspects of the work.

Ethics Approval and Consent to Participate

Not applicable.

Acknowledgment

Not applicable.

Funding

This study was supported by Natural Science Foundation of Chongqing (No. cstc2020jcyj-msxmX0630) and Chongqing medical scientific research project (Joint project of Chongqing Health Commission and Science & Technology Bureau) (No. 2019ZY3202).

Conflict of Interest

The authors declare no conflict of interest.

References

[1] Tan Z, Sun H, Xue T, Gan C, Liu H, Xie Y, *et al*. Liver Fibrosis: Therapeutic Targets and Advances in Drug Therapy. Frontiers in Cell and Developmental Biology. 2021; 9: 730176.

[2] Tsuchida T, Friedman SL. Mechanisms of hepatic stellate cell activation. Nature Reviews. Gastroenterology & Hepatology. 2017; 14: 397–411.

[3] Aydın MM, Akçalı KC. Liver fibrosis. The Turkish Journal of Gastroenterology. 2018; 29: 14–21.

[4] Bataller R, Brenner DA. Liver fibrosis. The Journal of Clinical Investigation. 2005; 115: 209–218.

[5] Asrani SK, Devarbhavi H, Eaton J, Kamath PS. Burden of liver diseases in the world. Journal of Hepatology. 2019; 70: 151–171.

[6] Seki E, Brenner DA. Recent advancement of molecular mechanisms of liver fibrosis. Journal of Hepato-Biliary-Pancreatic Sciences. 2015; 22: 512–518.

[7] Buyl K, Merimi M, Rodrigues RM, Moussa Agha D, Melki R, Vanhaecke T, *et al*. The Impact of Cell-Expansion and Inflammation on The Immune-Biology of Human Adipose Tissue-Derived Mesenchymal Stromal Cells. Journal of Clinical Medicine. 2020; 9: 696.

[8] El-Kehdy H, Najar M, De Kock J, Agha DM, Rogiers V, Merimi M, *et al*. Inflammation Differentially Modulates the Biological Features of Adult Derived Human Liver Stem/Progenitor Cells. Cells. 2020; 9: 1640.

[9] Berardis S, Lombard C, Evraerts J, El Taghdouini A, Rosseels V, Sancho-Bru P, *et al*. Gene expression profiling and secretome analysis differentiate adult-derived human liver stem/progenitor cells and human hepatic stellate cells. PLoS ONE. 2014; 9: e86137.

[10] Raicevic G, Najar M, Najimi M, El Taghdouini A, van Grunsven LA, Sokal E, *et al*. Influence of inflammation on the immunological profile of adult-derived human liver mesenchymal stromal cells and stellate cells. Cytotherapy. 2015; 17: 174–185.

[11] Lee YA, Wallace MC, Friedman SL. Pathobiology of liver fibrosis: a translational success story. Gut. 2015; 64: 830–841.

[12] Tian L, Tao ZZ, Ye HP, Li GY, Zhan ZF, Tuo HW. Overexpression of MEOX2 promotes apoptosis through inhibiting the PI3K/Akt pathway in laryngeal cancer cells. Neoplasma. 2018; 65: 745–752.

[13] Li X, Liu J, Gao T. beta-TrCP-mediated ubiquitination and degradation of PHLPP1 are negatively regulated by Akt. Molecular and Cellular Biology. 2009; 29: 6192–6205.

[14] Liu J, Weiss HL, Rychahou P, Jackson LN, Evers BM, Gao T. Loss of PHLPP expression in colon cancer: role in proliferation and tumorigenesis. Oncogene. 2009; 28: 994–1004.

[15] Liu P, Kong F, Wang J, Lu Q, Xu H, Qi T, *et al*. Involvement of IGF-1 and MEOX2 in PI3K/Akt1/2 and ERK1/2 pathways mediated proliferation and differentiation of perivascular adipocytes. Experimental Cell Research. 2015; 331: 82–96.

[16] Gurtner GC, Werner S, Barrandon Y, Longaker MT. Wound repair and regeneration. Nature. 2008; 453: 314–321.

[17] Higashi T, Friedman SL, Hoshida Y. Hepatic stellate cells as key target in liver fibrosis. Advanced Drug Delivery Reviews. 2017; 121: 27–42.

[18] Shang L, Hosseini M, Liu X, Kisseleva T, Brenner DA. Human hepatic stellate cell isolation and characterization. Journal of Gastroenterology. 2018; 53: 6–17.

[19] Tsochatzis EA, Bosch J, Burroughs AK. Liver cirrhosis. Lancet. 2014; 383: 1749–1761.

[20] Ying HZ, Chen Q, Zhang WY, Zhang HH, Ma Y, Zhang SZ, *et al*. PDGF signaling pathway in hepatic fibrosis pathogenesis and therapeutics (Review). Molecular Medicine Reports. 2017; 16: 7879–7889.

[21] Trojanowska M. Role of PDGF in fibrotic diseases and systemic sclerosis. Rheumatology. 2008; 47: v2–v4.

[22] Lim BJ, Lee WK, Lee HW, Lee KS, Kim JK, Chang HY, *et al*. Selective deletion of hepatocyte platelet-derived growth factor

receptor α and development of liver fibrosis in mice. Cell Communication and Signaling. 2018; 16: 93.

[23] Wang X, Gao Y, Li Y, Huang Y, Zhu Y, Lv W, *et al*. Roseotoxin B alleviates cholestatic liver fibrosis through inhibiting PDGF-B/PDGFR-β pathway in hepatic stellate cells. Cell Death & Disease. 2020; 11: 458.

[24] Lechuga CG, Hernández-Nazara ZH, Hernández E, Bustamante M, Desierto G, Cotty A, *et al*. PI3K is involved in PDGF-beta receptor upregulation post-PDGF-BB treatment in mouse HSC. American Journal of Physiology. Gastrointestinal and Liver Physiology. 2006; 291: G1051–G1061.

[25] Wang Y, Gao J, Zhang D, Zhang J, Ma J, Jiang H. New insights into the antifibrotic effects of sorafenib on hepatic stellate cells and liver fibrosis. Journal of Hepatology. 2010; 53: 132–144.

[26] Chen MH, Chen SH, Wang QF, Chen JC, Chang DC, Hsu SL, *et al*. The molecular mechanism of gypenosides-induced G1 growth arrest of rat hepatic stellate cells. Journal of Ethnopharmacology. 2008; 117: 309–317.

[27] Cunnington RH, Northcott JM, Ghavami S, Filomeno KL, Jahan F, Kavosh MS, *et al*. The Ski-Zeb2-Meox2 pathway provides a novel mechanism for regulation of the cardiac myofibroblast phenotype. Journal of Cell Science. 2014; 127: 40–49.

[28] Northcott JM, Czubryt MP, Wigle JT. Vascular senescence and ageing: a role for the MEOX proteins in promoting endothelial dysfunction. Canadian Journal of Physiology and Pharmacology. 2017; 95: 1067–1077.

[29] Ávila-Moreno F, Armas-López L, Álvarez-Moran AM, López-Bujanda Z, Ortiz-Quintero B, Hidalgo-Miranda A, *et al*. Overexpression of MEOX2 and TWIST1 is associated with H3K27me3 levels and determines lung cancer chemoresistance and prognosis. PLoS ONE. 2014; 9: e114104.

[30] Armas-López L, Piña-Sánchez P, Arrieta O, de Alba EG, Ortiz-Quintero B, Santillán-Doherty P, *et al*. Epigenomic study identifies a novel mesenchyme homeobox2-GLI1 transcription axis involved in cancer drug resistance, overall survival and therapy prognosis in lung cancer patients. Oncotarget. 2017; 8: 67056–67081.

[31] Li X, Stevens PD, Yang H, Gulhati P, Wang W, Evers BM, *et al*. The deubiquitination enzyme USP46 functions as a tumor suppressor by controlling PHLPP-dependent attenuation of Akt signaling in colon cancer. Oncogene. 2013; 32: 471–478.